Molecular Therapy
Methods & Clinical Development
Original Article

Design and validation of cell-based potency assays for frataxin supplementation treatments

Shibani Mukherjee,[1] Larisa Pereboeva,[2] Daniel Fil,[3] Achisha Saikia,[1,4] Jeon Lee,[4] Jixue Li,[1] M. Grazia Cotticelli,[5] Elisabetta Soragni,[6] Robert B. Wilson,[5] Marek Napierala,[1] and Jill S. Napierala[1]

[1]Department of Neurology, O'Donnell Brain Institute, University of Texas Southwestern Medical Center, 6000 Harry Hines Boulevard, Dallas, TX 75390, USA; [2]Department of Biochemistry and Molecular Genetics, University of Alabama at Birmingham, 1825 University Boulevard, Birmingham, AL 35294, USA; [3]Department of Biochemistry and Molecular Biology, University of Arkansas for Medical Sciences, Little Rock, AR 72205, USA; [4]Lyda Hill Department of Bioinformatics, University of Texas Southwestern Medical Center, 5323 Harry Hines Boulevard, Dallas, TX 75390, USA; [5]Department of Pathology and Laboratory Medicine, Children's Hospital of Philadelphia, Philadelphia, PA 19104, USA; [6]Friedreich's Ataxia Research Alliance, 533 W. Uwchlan Avenue, Downingtown, PA 19335, USA

Friedreich's ataxia (FRDA) is a multisystem, autosomal recessive disorder caused by mutations in the frataxin (*FXN*) gene. As FRDA is considered an FXN deficiency disorder, numerous therapeutic approaches in development or clinical trials aim to supplement FXN or restore endogenous *FXN* expression. These include gene therapy, protein supplementation, genome editing or upregulation of *FXN* transcription. To evaluate efficacy of these therapies, potency assays capable of quantitative determination of FXN biological activity are needed. Herein, we evaluate the suitability of mouse embryonic fibroblasts derived from Fxn G127V knockin mice (MUT MEFs) as a candidate for cell-based potency assays. We demonstrate that these cells, when immortalized, continue to express minute amounts of Fxn and exhibit a broad range of phenotypes that result from severe Fxn deficiency. Exogenous FXN supplementation reverses these phenotypes. Thus, immortalized MUT MEFs are an excellent tool for developing potency assays to validate novel FRDA therapies. Care needs to be exercised while utilizing these cell lines, as extended passaging results in molecular changes that spontaneously reverse FRDA-like phenotypes without increasing Fxn expression. Based on transcriptome analyses, we identified the Warburg effect as the mechanism allowing cells expressing a minimal level of Fxn to thrive under standard cell culture conditions.

INTRODUCTION

Friedreich's ataxia (FRDA) is the most common hereditary ataxia. Symptoms typically appear in childhood or adolescence and include ataxia, loss of deep tendon reflexes, and hypertrophic cardiomyopathy. FRDA is a relentlessly progressive, life-shortening disorder caused by mutations in the frataxin (*FXN*) gene that significantly decrease FXN levels.[1–3] Most FRDA patients carry homozygous expansions of GAA repeats in intron 1 of *FXN*, while ~4% are compound heterozygous and carry a GAA expansion on one allele and a point mutation on the second *FXN* allele.[4,5] Frataxin is a small mitochondrial protein important for the biosynthesis of iron-sulfur (Fe-S) clusters, thus its deficit results in pleiotropic consequences for cellular metabolism ranging from lowered energy production to deficient DNA repair.[6]

There are two general strategies for FRDA therapy: directly targeting FXN deficiency or targeting cellular consequences of low FXN levels. Recently, the NRF2 agonist omaveloxolone (Skyclarys) was approved as a treatment to slow FRDA symptom progression.[7–9] The potentially most impactful approaches being developed aim to increase the level of FXN. Gene therapy, protein replacement strategies, approaches to reactivate endogenous *FXN* transcription, stabilize *FXN* mRNA, boost FXN translation or remove expanded GAA repeats all hold promise of targeting the very core of the disease.[10–14] Success of the above-mentioned strategies depends on developing two seemingly simple assays: first, to reliably and quantitatively measure FXN levels in peripheral tissues and, second, to demonstrate the biological activity and efficacy of the therapy leading to FXN increase. Measuring biological activity of FXN increase is connected to the development of a robust potency assay. This is a necessary step during design, validation, production, and storage of practically any gene therapy or protein supplementation product.[15,16] The development of a quantitative method to measure potency allows comparison of the drug to a reference standard and is used to verify that only product lots with attributes that meet appropriate quality control standards are employed during drug clinical development and following market approval. Potency is defined as the quantitative measure of biological activity related to a relevant biological function of a product.[15,16] Thus, for FRDA, the targeted biological activity should be related to any of the pleiotropic functions of FXN. For example, pathological downregulation of FXN leads to deficient Fe-S cluster biogenesis, which in turn manifests in decreased oxidative phosphorylation, decreased activity of tricarboxylic acid (TCA) cycle enzymes relying

Received 28 June 2024; accepted 24 September 2024;
https://doi.org/10.1016/j.omtm.2024.101347.

Correspondence: Jill S. Napierala, Department of Neurology, O'Donnell Brain Institute, University of Texas Southwestern Medical Center, 6000 Harry Hines Boulevard, Dallas, TX 75390, USA.
E-mail: jill.napierala@utsouthwestern.edu

Published by Elsevier Inc. on behalf of The American Society of Gene and Cell Therapy.
This is an open access article under the CC BY-NC-ND license (http://creativecommons.org/licenses/by-nc-nd/4.0/).

on Fe-S cofactors, decreased overall energy output, and increased oxidative stress.[17–21]

Potency assays can be developed using *in vivo* animal models, cell-based systems, or *in vitro* assays.[6,22] Cellular disease models offer an economical advantage but may suffer from issues related to variability and to changes in cell lines over time due to acquired mutations or genetic drift. Commonly utilized cellular models of FRDA are patient-derived, immortalized lymphoblastoid cell lines, primary skin fibroblasts, and induced pluripotent stem cell (iPSC)-differentiated cells, such as neurons or cardiomyocytes.[23–27] While all of these cell types demonstrate molecular features of FRDA (GAA repeat expansion, decreased *FXN* expression, chromatin changes at the *FXN* locus), their cellular phenotype is not very robust or reproducible.[28–31] Other frequently used FRDA cellular models rely on GAA-independent FXN depletion mediated by small interfering/short hairpin RNAs. While associated with severe phenotypes, these cell lines do not fully recapitulate FRDA pathology likely due to the sudden and dramatic decrease of FXN.[32–35]

Here, we developed new cellular potency assays using FRDA mouse model cells that harbor homozygous missense point mutations in the *Fxn* gene. We derived mouse embryonic fibroblasts (MEFs) from Fxn G127V mutant mice established by our group.[36] The G127V mutation in Fxn corresponds to the human FXN G130V mutation, the most frequent point mutation found in FRDA patients. The G127V MEFs (termed MUT hereafter) express extremely low levels of G127V Fxn (~1% of wild-type [WT] levels) and exhibit robust cellular phenotypes: decreased growth rate, decreased intracellular ATP levels, and elevated reactive oxygen species (ROS) levels when compared with WT MEFs.[36,37] These strong phenotypes result in a very limited proliferation capacity of MUT MEFs (3–5 passages), making their direct use impossible without constant derivation of new cells from G127V MUT animals. Therefore, we immortalized MUT MEFs using retrovirally encoded Simian virus 40 large T antigen (SV40 T_{ag}) and demonstrated that early passages of immortalized MUT MEFs hold promise as a valuable cellular model for conducting potency assays in the process of FRDA drug development and production.

RESULTS

SV40 T antigen-mediated immortalization of MUT MEFs does not affect Fxn expression

To develop a potency assay for FRDA supplementation therapies, we utilized MEFs derived from Fxn G127V mice. These primary cells, expressing an extremely low level (~1%) of Fxn compared with WT MEFs, showed dramatically decreased proliferation and increased cellular senescence.[36] As MUT MEFs ceased to proliferate after ~4 passages in normoxic conditions, we immortalized these cells using overexpression of SV40 T_{ag}. The gene encoding T_{ag} was delivered to both WT and MUT cells using retroviral transduction, under puromycin selection. MEF lines independently derived from two WT embryos and two MUT embryos were selected for immortalization (Figure 1A). As random integration of the SV40 transgene can result in variable T antigen expression levels, we decided to isolate individual, single-cell-derived clones from each of the immortalized MEF lines. SV40 T_{ag} and Fxn protein levels in clones from one WT line

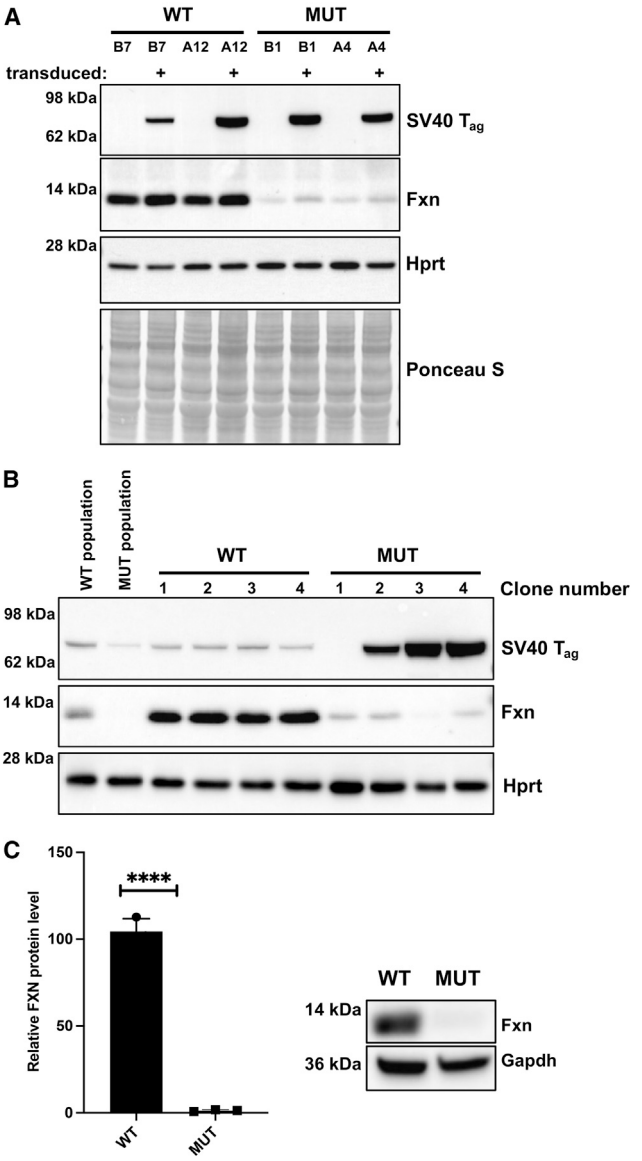

Figure 1. Immortalization of MUT MEFs with SV40 T antigen does not affect Fxn expression

(A) Expression of Fxn and SV40 T_{ag} in immortalized WT and MUT MEFs (populations) as shown by western blot. Hprt and Ponceau S staining serve as loading controls. SV40 transformation was conducted on two independently derived WT MEF lines (B7, A12) and two independently derived MUT MEF lines (B1, A4). Non-transduced cell lines are shown for reference. (B) Expression of Fxn, SV40 T_{ag}, and Hprt in the selected single-cell derived clones shown by western blot. (C) Quantitation of Fxn expression in selected clones (#3 WT and #4 MUT), which were used for further experiments. Gapdh was used as a loading control. A representative western blot is shown. Western blots were performed three independent times. Results are plotted as mean values with standard deviations; (****$p < 0.0001$).

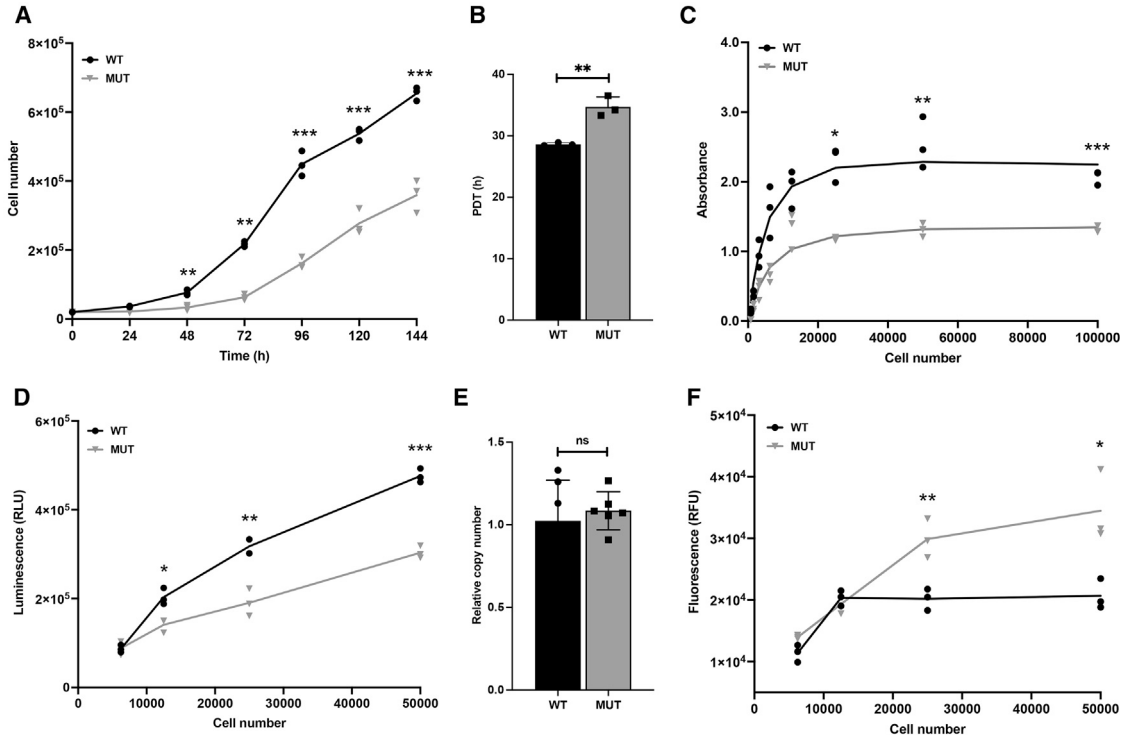

Figure 2. Immortalized WT and MUT MEFs cells are phenotypically different

(A) Immortalized WT and MUT MEFs were seeded at the same density and counted every 24 h over a 6-day period. The experiment was conducted independently three times. (B) The PDTs of WT and MUT MEFs were calculated from the growth curves (A) as described in the materials and methods section. Results are plotted as mean values with standard deviations. (C) Cell proliferation assays were independently performed three times. (D) WT and MUT MEFs were plated at densities indicated by the x axis and analyzed for intracellular ATP content 48 h later by luminescence detection (y axis). Three independent experiments were performed. (E) Determination of mitochondrial DNA copy number by qPCR in WT and MUT MEFs. Experiments were done on six independently cultured samples. Results are plotted as mean values with standard deviations. (F) The level of ROS in immortalized WT and MUT MEFs plated at the indicated densities (x axis) was measured by staining the cells with the fluorescent ROS indicator CM-H_2DCFDA. The experiments were independently performed three times. Symbols denote statistical significance as follows: $^{**}p < 0.001$, $^{***}p < 0.0001$.

(A12) and one MUT line (A4) are shown in Figure 1B. Interestingly, most MUT clones showed higher expression of the SV40 T_{ag} compared with WT clones. Importantly, expression of SV40 T_{ag} did not increase endogenous Fxn protein expression in MUT cells (Figures 1B and 1C). Further experiments were conducted using clonally derived WT and MUT SV40-transformed MEFs.

Immortalized MUT and WT MEFs are phenotypically different

We next examined the cellular growth rate of WT (clone # 3) and MUT (clone #4) MEF cells (Figure 1B). We found that the rate of cell growth was significantly slower in MUT cells (Figure 2A). The population doubling time (PDT) time was approximately 26–28 h and 33–36 h for WT and MUT cells, respectively (Figure 2B). This difference in growth was also apparent in cell proliferation assays (Figure 2C). Deficiency of FXN has been shown to affect intracellular ATP levels.[38,39] A luminescent assay for intracellular ATP levels showed a significantly lower level of ATP in MUT compared with the WT MEFs (Figure 2D), without affecting mitochondrial DNA copy number (Figure 2E). Next, to determine the level of oxidative stress in the MUT MEFs, we measured accumulation of ROS in live cells using the fluorescent indicator CM-H_2DCFDA. We found that the intracellular level of ROS was significantly higher in MUT cells than in WT MEFs (Figure 2F). This is consistent with previous studies that have shown that FXN deficiency can increase oxidative stress.[38,40] We confirmed these results in a second, independently isolated pair of MUT and WT clones (Figure S1). In summary, our results suggest that immortalized MUT MEFs have a lower proliferation rate, decreased amount of ATP, and a higher oxidative stress level than WT MEFs. This indicates that the expression of SV40 T_{ag} did not change the characteristics of primary, non-immortalized MEFs.[36]

Partial reversal of abnormal phenotype in MUT cells via exogenous FXN expression

The human *FXN* coding sequence, including a fragment of the *FXN* 5′ UTR and truncated intron 1 (miniFXN7)[41] was cloned into a lentivirus expression vector (Figure 3A). Subsequently, SV40-immortalized MUT cells were transduced with lentivirus expressing FXN at an early passage (p6) and selected with Hygromycin B. Western blot analyses demonstrated that the level of exogenous FXN expression in MUT MEFs is similar to the amount of Fxn detected in WT MEFs (Figures 3B and 3C). Next, we determined the growth rate of WT, MUT, and MUT+FXN MEFs (Figure 4). As expected, exogenous

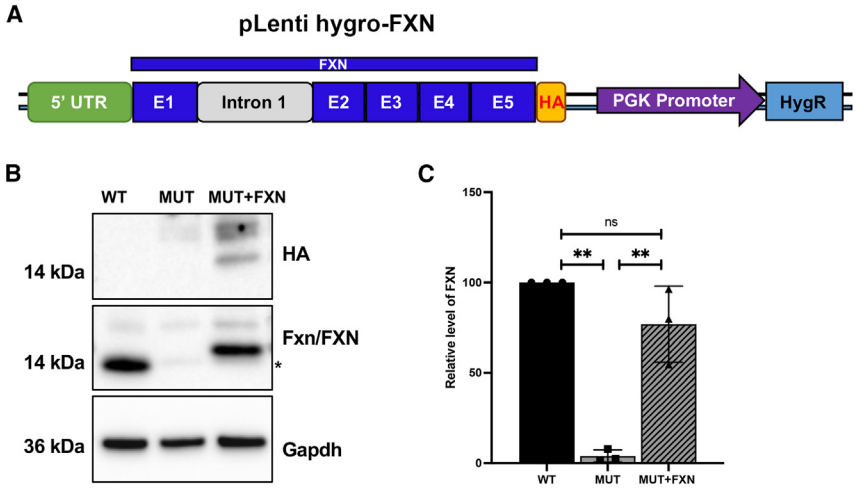

Figure 3. Stable expression of exogenous human FXN in MUT MEFs

(A) A schematic of the lentivirus vector pLenti hygro FXN encoding a human miniFXN gene. The miniFXN gene used in experiments contains fragments of the endogenous *FXN* 5′UTR, promoter and intron 1, and all five exons of the gene. (B) Representative western blot demonstrating expression of exogenous FXN. The miniFXN encodes a C-terminal HA tag that results in a slightly greater molecular weight, as detected by western blot. (C) Quantitation of endogenous Fxn (*) and exogenous FXN by western blot. Gapdh was used as a normalization control. MUT+FXN designates cells expressing exogenous, human FXN. The experiment was performed three independent times. Results are plotted as mean values with standard deviations; (**$p < 0.001$, ***$p < 0.0001$).

expression of FXN led to increased proliferation rate of MUT MEFs when compared with parental cells (Figure 4A). The PDT for MUT+FXN cells was ∼29–31 h, significantly shorter than MUT cells (∼41–42 h) but longer than WT MEFs (∼23–26 h; Figure 4B). Similarly, the cell proliferation assay showed that the proliferation rate of MUT+FXN cells was intermediate between WT and MUT MEFs (Figure 4C). In addition, exogenous FXN expression in the MUT+FXN MEFs was sufficient to increase the ATP level and significantly lower oxidative stress to the levels observed in WT cells (Figures 4D and 4E). In summary, these results suggest that supplementation with exogenous FXN can partially rescue the FRDA-like phenotypes in immortalized MUT MEFs.

Extended passaging alters phenotypes of immortalized MUT MEFs

Surprisingly, we noted a significant acceleration of growth rate after continuous passaging of SV40 immortalized MUT MEFs (p19–p26; long-term [-LT]). Indeed, the PDT for early-passage MUT MEFs decreased over time to the PDT observed for WT MEFs of similar passage (∼23–26 h, Figures 5A and 5B). Likewise, no statistical differences were observed between late-passage MUT-LT and WT cells for proliferation, as measured by cell proliferation assays (Figure 5C), nor for ATP and cellular ROS levels (Figures 5D and 5E). Importantly, this phenotypic shift occurred without any alteration in Fxn levels in MUT-LT MEFs compared with early-passage MUT cells (Figure 5F). These results were validated in an additional pair of MUT and WT clonal MEF lines (Figure S2). Collectively, these data suggest that immortalized MUT cells can adapt to the expression of extremely low levels of Fxn and change their phenotype to resemble WT cells expressing higher levels of Fxn.

Differential gene expression analysis reveals gross transcriptome differences between early and late passage of MUT MEFs

To decipher molecular mechanisms underlying the phenotypic changes observed in MUT-LT MEFs, we conducted a comparative transcriptome analysis of WT, MUT, and MUT-LT cells (Figure 6A). RNA sequencing (RNA-seq) revealed that 1,937 genes (834 downregulated and 1,103 upregulated) displayed differential expression (DE) between early-passage WT and MUT MEFs. This represents a significantly higher number of DE genes than observed between early-passage WT and MUT-LT cells (455 DE genes; 212 downregulated and 243 upregulated; Figure 6B). Principal-component analysis (PCA) underscored the significant deviation of MUT-LT MEFs from their early-passage characteristics, yet they still did not perfectly group with WT MEFs (Figure 6C). Utilizing the DAVID functional annotation tool, we explored Kyoto Encyclopedia of Genes and Genomes (KEGG) pathways altered in early-passage MUT MEFs compared with WT. We found that ribosomal biosynthesis, tRNA metabolism, and several other translation-related pathways were significantly downregulated in early-passage MUT cells (Table S1). Numerous ribosomal protein L and S (*Rpl* and *Rps*) genes were expressed at lower levels in early-passage MUT MEFs than in WT and MUT-LT MEFs (Figure S3). Furthermore, we did not observe any changes in the protein translation-related pathways between MUT-LT and WT cells (Table S2). Increased expression of genes associated with translation would explain the increased proliferative capacity of MUT-LT cells. SV40 T_{ag} expression can affect cellular metabolism, especially pathways responsible for energy production. Therefore, we examined expression of major genes associated with glucose metabolism, the primary carbon source of cultured MEFs. Interestingly, we identified upregulated expression of several genes involved in aerobic glycolysis (also known as the Warburg effect) in MUT-LT MEFs when compared with early-passage cells (Figure 7). These included glucose transporter solute carrier family 2, member 1 (*Slc2a1*) and lactate dehydrogenase A (*Ldha*), proteins critically involved in glucose utilization. In summary, RNA-seq analysis revealed that MUT-LT MEFs alter their transcriptome during prolonged time in culture, likely affecting intracellular metabolism. This suggests that these cells may be transitioning from an MUT to WT growth phenotype, even while maintaining low levels of Fxn.

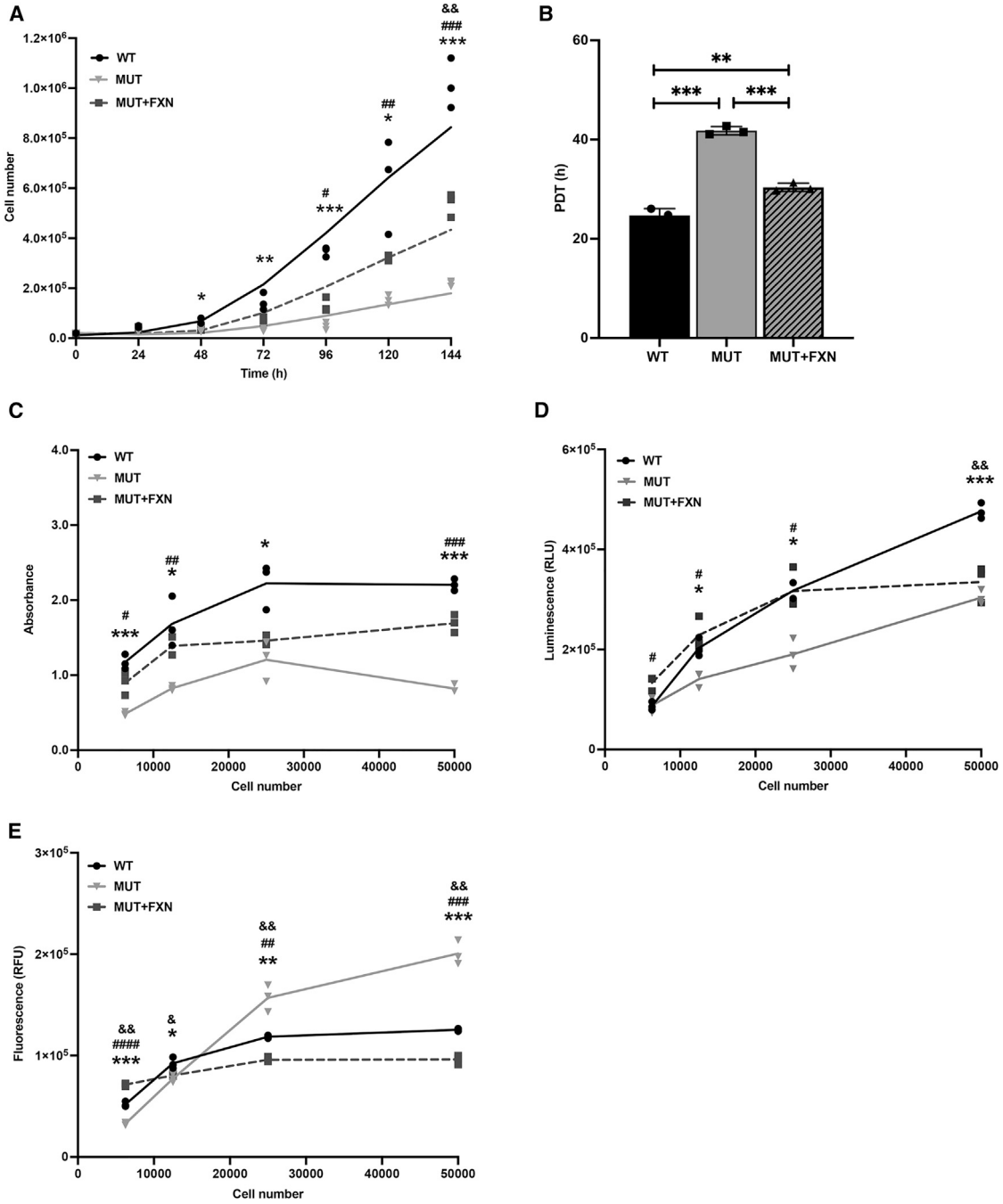

Figure 4. Exogenous FXN expression ameliorated aberrant phenotypes of MUT MEFs

(A) Immortalized WT, MUT, and MUT+FXN MEFs were seeded at the same density and counted every 24 h over a 6-day period. The experiment was conducted independently three times. (B) The PDTs of WT, MUT, and MUT+FXN were calculated from the growth curves (A). Results are plotted as mean values with standard deviations. (C) Proliferation of WT, MUT, and MUT+FXN MEFs was assessed using cell proliferation assays. Cells were plated at the indicated densities independently for three separate experiments. (D) WT, MUT, and MUT+FXN MEFs were plated at the densities indicated by the x axis and analyzed for intracellular ATP content 48 h later by luminescence detection (y axis). Three independent experiments were performed. (E) The level of ROS in WT, MUT, and MUT+FXN MEFs was determined using CM-H_2DCFDA labeling. Symbols denote statistical significance as follows: $^{*, \#, \&}p < 0.05$, $^{**, \#\#, \&\&}p < 0.001$, $^{***, \#\#\#, \&\&\&}p < 0.0001$. *WT vs. MUT, $^{\#}$MUT vs. MUT+FXN, $^{\&}$WT vs. MUT+FXN.

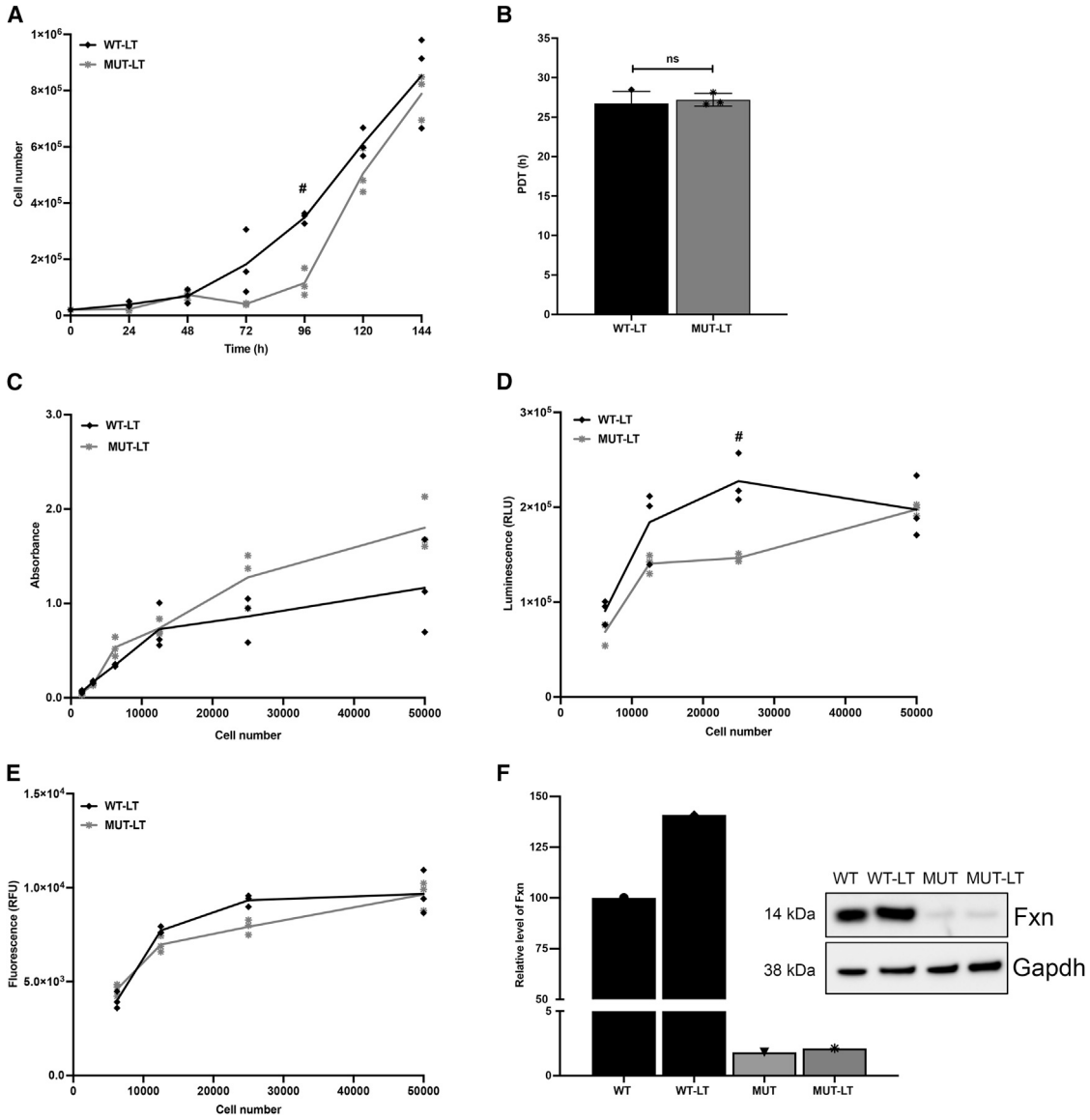

Figure 5. Prolonged culturing partially alleviates MUT MEF phenotypes

(A) Immortalized late-passage WT (WT-LT, p26) and MUT (MUT-LT, p26) MEFs were seeded at the same density and counted every 24 h over a 6-day period. The experiment was performed independently three times. (B) The PDTs of WT-LT and MUT-LT MEFs were calculated from the growth curves (A). Results are plotted as mean values with standard deviations. (C) Proliferation of immortalized WT-LT and MUT-LT was compared using cell proliferation assays. Cells were plated at the indicated densities (x axis) independently for three separate experiments. (D) WT-LT and MUT-LT MEFs were plated at the densities indicated by the x axis and analyzed for intracellular ATP content 48 h later by luminescence detection (y axis). The experiment was performed independently three times. (E) The level of ROS in WT-LT and MUT-LT MEFs was measured by fluorescent detection (y axis) after staining the cells with CM-H_2DCFDA. Cells were plated at the indicated densities (x axis) independently for three separate experiments (**$p < 0.001$, ***$p < 0.0001$). (F) FXN protein levels were measured by western blot in WT, WT-LT, MUT, and MUT-LT MEFs. Gapdh was used as a loading control and normalizer.

DISCUSSION

The goal of this study was to develop a reliable potency assay for FRDA gene or protein replacement therapies. We utilized MEFs derived from Fxn G127V mice because they express minimal levels of Fxn (~1% in MEFs) and demonstrate robust, measurable phenotypes.[36,37] In fact, while homozygous Fxn G127V/G127V mice are viable, hemizygous G127V/null animals are not, indicating that further decrease of Fxn by 50% is incompatible with life. Such low levels of Fxn as detected in MUT cells have never been observed in any other currently available cellular models of the disease (lymphoblasts, fibroblasts, iPSCs, and their differentiated progeny, or cells derived from other FRDA mouse models). Furthermore,

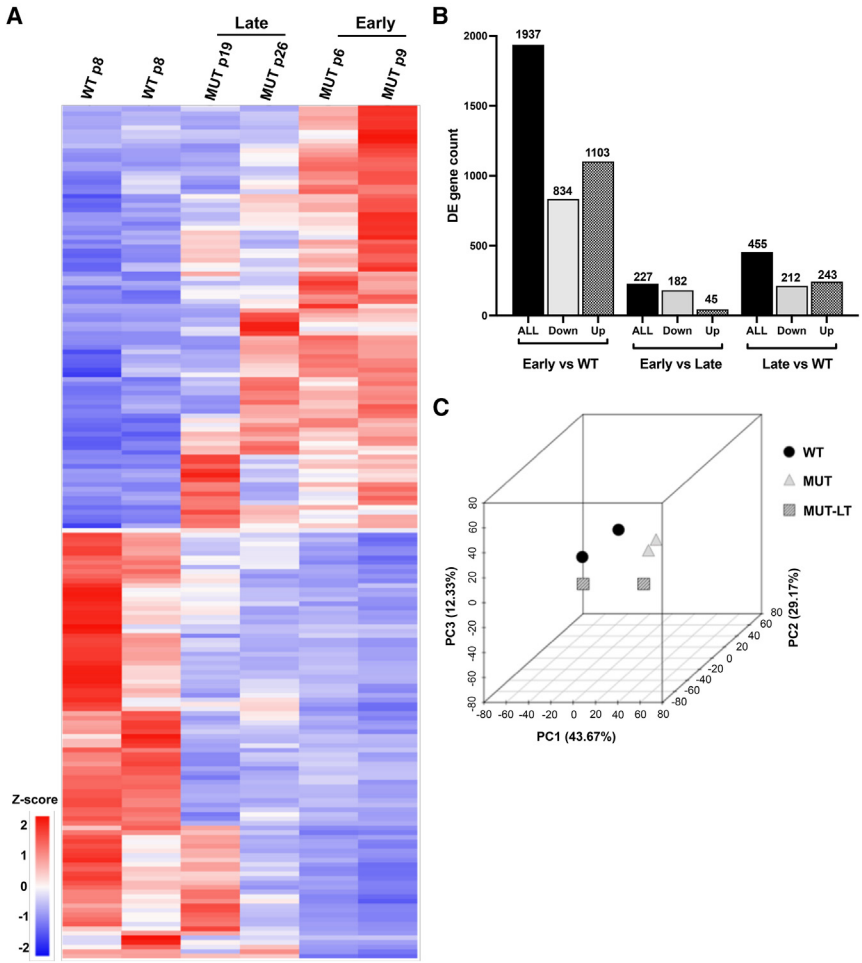

Figure 6. Changes of transcriptome associated with prolonged culture of MUT MEFs

(A) Heatmap illustrating expression of 2017 DE genes in WT, MUT-LT, and MUT early-passage MEFs. p indicates passage number. (B) Numbers of significantly DE genes separated by direction of change (all, upregulated, downregulated) and organized by group comparison ($p < 0.05$). Early indicates early-passage MUT cells (p6 and p9); Late indicates late-passage MUT cells (p19 and p26). (C) Principal-component analysis (PCA) of early-passage WT and early-passage MUT MEF samples and MUT-LT MEF samples.

immortalization of MUT cells via SV40 T_{ag} expression did not change their fundamental characteristics during initial passages. Importantly, exogenous expression of physiological levels of human FXN in the immortalized MUT MEFs partially corrected phenotypes, demonstrating that these cells could serve as an appropriate cellular model for FRDA potency assays. Incomplete rescue could be explained by several factors; the relatively short period of time between FXN expression and phenotype measurement, the presence of a C-terminal HA epitope tag or the modest expression level of FXN elicited by our expression method. These possibilities are not mutually exclusive, but do not preclude the conclusion that exogenous FXN expression was sufficient to mitigate the established cellular phenotypes. The miniFXN gene encoding the endogenous human *FXN* promoter along with a fragment of intron 1 and the remaining *FXN* coding sequence was selected to ensure moderate FXN expression. However, the MUT cells also could be utilized for testing various *FXN* promoters and potential cellular consequences of FXN overexpression.

While untransformed MUT MEFs rapidly senesce after a few passages, SV40-transduced cells are capable of continuous proliferation despite unchanged (low) levels of Fxn. However, the growth rate of immortalized MUT MEFs increases with continuous passage. RNA-seq analyses of early-passage WT, and early- and late-passage MUT MEFs revealed dramatic changes in the transcriptome of MUT-LT cells compared with the early-passage cells. As expected, rapid proliferation was associated with increased synthesis of ribosomal RNA and tRNA synthesis genes[42–44] as necessary to increase production of cellular proteins. In addition, we detected changes in the expression of genes important for energy production and glucose utilization in MUT-LT cells, suggesting metabolic reprogramming of the early-passage MUT MEFs over time. We found that several genes associated with aerobic glycolysis, also referred to as the Warburg effect, are upregulated in MUT-LT cells. Aerobic glycolysis is the conversion of glucose to lactate that occurs in an oxygen-rich environment. It is a process frequently used by cancer cells, along with intact oxidative phosphorylation, to increase cellular energy production.[45–49] Beyond ATP production, aerobic glycolysis yields a rich pool of carbon intermediates that are used for nucleotide, lipid, and protein biosynthesis to promote cell survival and proliferation.[50,51] Finally, aerobic glycolysis decreases ROS production and oxidative damage, typically associated with mitochondrial respiration, thus protecting cells from apoptosis.[52]

While WT cells may utilize both oxidative phosphorylation and glycolysis, FRDA cells, including MUT, are disadvantaged for energy production via oxidative phosphorylation because low FXN/Fxn levels are associated with decreased biosynthesis of Fe-S clusters, which in turn inhibits activities of Complexes I–III.[53–57] However, the metabolic shift that occurs during extended culture of immortalized G127V MUT cells differs from shifts described for other FRDA cellular models.[58–60] MUT cells are not predisposed toward glycolysis in their untransformed state, rather they rely mostly on fatty acid oxidation for energy production.[36] It is only after SV40-mediated immortalization that MUT MEFs shift their metabolic program toward aerobic glycolysis. Thus, SV40-immortalized MUT cells cultured over time in normoxic (oxygen-rich) conditions, like those

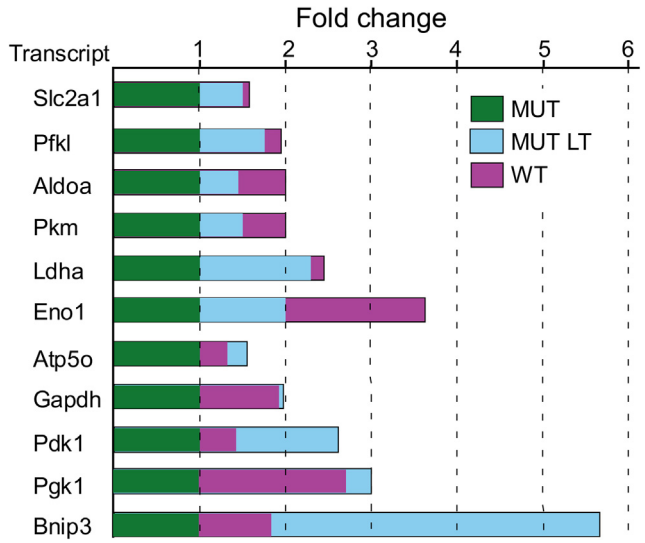

Figure 7. Upregulated expression of aerobic glycolysis (Warburg effect) associated genes in MUT-LT cells

Normalized RNA-seq counts were used to generate the plot. All values were normalized to the expression level detected in early-passage MUT cells (MUT, green bar; MUT-LT, blue bar; WT, purple bar).

utilized in our study, likely adapt to predominantly depend on aerobic glycolysis to fulfill energy and biomass requirements for survival in their transformed state. This metabolic reprogramming is probably initiated by expression of SV40 T_{ag} during the immortalization process. For example, SV40 T_{ag} could facilitate the adaptive mechanism via deactivation (or sequestration) of *Trp53* (p53 tumor suppressor), resulting in upregulation of glucose transporter expression (e.g., *Slc2a1*).[61,62]

In summary, MUT cells are unique in that they are viable while expressing an extremely low level of Fxn. Our data demonstrate that they could be an appropriate model for cell-based potency assays. However, following immortalization, their metabolic adaptability makes it necessary to strictly monitor for potential drift of proliferation-dependent phenotypes. While several studies indicated specific sensitivity of FRDA cells to different carbon sources, systematic investigation are lacking. The low Fxn level in MUT cells and consequently their phenotype could be a very sensitive system to empirically dissect metabolic pathways that are the most affected in FRDA.

MATERIALS AND METHODS

Culture and immortalization of MEFs

Mouse embryonic fibroblasts (MEFs) were derived from both WT and G127V mutant (MUT) mice as described previously.[36] These MEFs were cultured in Dulbecco's modified Eagle's medium (DMEM) with high-glucose and pyruvate (Life Technologies, #11995), supplemented with 10% fetal bovine serum (HyClone, #SH30396.03). Immortalization of WT and MUT cells was achieved using an SV40 immortalization kit (Alstem, #CILV01) according to the manufacturer's recommendations. Early passages were defined as passages 6–14, while late passages encompassed passages 15–26.

Growth curves and population doubling time of MEFs

MEFs were seeded in triplicate in 12-well plates at a density of 2×10^4 cells per well and cultured in a standard cell culture incubator (37°C, 5% CO_2). Cells were detached with trypsin and counted daily from days 1–8 after seeding. Population doubling time was calculated during the logarithmic phase of growth using the formula: $PDT = T \times \ln(2)/\ln(A/A_0)$, where T represents the duration of culture in hours (h), A corresponds to the number of cells in the well at the time of measurement, and A_0 denotes the initial number of cells.

Cell proliferation assay

MEFs were seeded at varying cell densities (ranging from 5×10^3–1×10^5 cells per well) in 96-well plates. After 48 h, cells were incubated with XTT (sodium 2,3,-bis(2-methoxy-4-nitro-5-sulfophenyl)-5-[(phenylamino)-carbonyl]-2H-tetrazolium); ATCC, #30-1011K) for 2–3 h. Absorbance of wells containing cells (test) and media only (blank) was recorded at 465 and 660 nm using a BMG Biotech FLUOstar Omega plate reader. Specific absorbance was calculated according to the following formula:

$$\text{Specific Absorbance} = A_{465\text{nm(Test)}} - A_{465\text{nm(Blank)}} - A_{660\text{nm(Test)}}$$

Quantitation of mRNA

RNA was isolated from MEFs using the RNeasy Mini Kit (Qiagen, #74104) followed by removal of genomic DNA contamination using the TURBO DNA-free Kit (Invitrogen, #AM1907). The expression of *Fxn* and *Gapdh* (normalizer) transcripts was quantitated by Power SYBR Green RNA-to-CT 1-Step Kit (Applied Biosystems, #4389986) using primers and conditions as described.[36]

Quantification of mitochondrial copy number

Relative mtDNA copy number was determined as described.[36] Briefly, total DNA was isolated with the QIAamp DNA Mini Kit (Qiagen, #51304) according to the manufacturer's instructions. A short mtDNA fragment (16S rRNA gene, mt-Rnr2) was quantified with Power SYBR Green PCR (Thermo Fisher Scientific, #4367659) relative to genomic DNA (hexokinase 2 gene, *Hk2*). The sequence of the primers and reactions condition were described in Fil et al.[36]

Western blot

For total protein isolation, MEFs were lysed in buffer (0.1% NP-40, 0.25 M sodium chloride, 5 mM ethylenediaminetetraacetic acid, 50 mM HEPES, pH 7.5) supplemented with 1 mM dithiothreitol and 1% protease inhibitor cocktail (Sigma-Aldrich, #P8340). Following incubation on ice for 20 min, samples were centrifuged at 20,000 × *g* for 10 min at 4°C. The soluble fraction was collected, and protein concentration was determined using the Bradford Protein Assay Reagent (Bio-Rad, #5000006). Subsequently, protein samples were heated with reducing sample buffer (50 mM Tris-HCl, pH 6.8, 2% SDS, 0.1% bromophenol blue, 10% glycerol, 100 mM DTT) at

95°C and resolved on 4%–12% NuPAGE Bis-Tris gels, followed by transfer to nitrocellulose membranes. Membranes were blocked with 5% milk in Tris-buffered saline (TBST; 10 mM Tris-HCl, pH 7.5, 150 mM NaCl, 0.1% Tween 20) and probed with primary antibodies for frataxin/Frataxin (Proteintech, #14147-1-AP), Hprt (Proteintech, #15059-1-AP), Gapdh (Millipore, #MAB374), followed by incubation with secondary antibodies, either anti-Rabbit HRP linked (GE Healthcare, #NA934V) or anti-Mouse HRP linked, (GE Heatlhcare, #NA931V). Signal was detected using SuperSignal West Dura Extended Duration Substrate (Thermo Fisher Scientific, #34075) or SuperSignal West Femto Maximum Sensitivity Substrate (Thermo Fisher Scientific, #34095). Imaging and analysis were performed with a Bio-Rad ChemiDoc MP Imaging System using ImageLab v.6.0.1 software.

ROS measurement

MEFs were seeded at 5×10^3–5×10^4 cells per well in 96-well plates and cultured for 48 h, followed by incubation with General Oxidative Stress Indicator CM-H_2DCFDA (Invitrogen, #C6827) for 40 min. Fluorescence was measured using BMG Biotech FLUOstar Omega plate reader at Ex/Em = 485/535 nm in endpoint mode.

ATP measurement

MEFs were seeded at 5×10^3–5×10^4 cells per well in 96-well plates and cultured for 48 h. ATP levels were measured using the Luminescent ATP Detection Assay Kit (Abcam, #ab113849) following the manufacturer's recommendations.

Cloning and packaging of pLenti hygro FXN-L

A miniFXN construct expressing human *FXN* under the control of endogenous regulatory elements was cloned into the pLenti HRE-Luc pGK Hygro (Addgene plasmid #118706). A fragment of 2,782 base pairs (bp) containing the entire *FXN* gene was excised from pAAV FXN-L using *Mlu*I, *Pml*I, and *Aat*I restriction enzyme digestion and cloned into pLenti HRE-Luc pGK Hygro digested with *Mlu*I and *Pme*I. Lentivirus packaging was performed in HEK293 cells using pMD2.G (Addgene #12259) and psPAX2 (Addgene #12260), together with the pLenti hygro FXN-L. Viral titers were determined using the Lenti-X qRT-PCR Titration Kit (Takara, #631235).

RNA sequencing analysis

Total RNA was extracted from two clones each of early-passage WT, MUT, and late-passage MUT cell lines using the RNeasy Mini Kit (Qiagen, #74104) followed by removal of genomic DNA contamination using the TURBO DNA-free Kit (Invitrogen, #AM1907). Sequencing libraries were generated at Novogene Co., Ltd using NEBNext Ultra RNA Library Prep Kit for Illumina (NEB, #E7770) following manufacturer's recommendations. Library quality was assessed on the Agilent Bioanalyzer 2100 system. Cluster generation and sequencing were performed on Illumina's NovaSeq6000 S4 flow cell to yield 20 million paired-end reads (PE150) per sample. Quality filtered reads were aligned to the mouse genome with HISAT2 and quantified. Differential gene expression analyses were performed using DESeq2.[63] Genes were considered differentially expressed if their adjusted p value was less than 0.05, and the absolute value of their log 2-fold change exceeded 0. The DAVID functional annotation tool (https://david.ncifcrf.gov/tools.jsp) and the KEGG pathway database (https://www.genome.jp/kegg/pathway.html) were used for pathway analyses. RNA-seq data are available in the GEO database (accession #GSE255810).

Statistical analyses

Statistical analyses were performed using GraphPad Prism v.9. Student's unpaired, two-tailed t tests, multiple t tests with two-stage step-up (Benjamini, Krieger, and Yekutieli), and ordinary one-way ANOVA for multiple comparisons were employed to determine statistical significance, with a threshold of $p < 0.05$ considered significant.

DATA AND CODE AVAILABILITY

The raw and processed RNA-seq data generated in this study will be deposited in the Gene Expression Omnibus under accession number GSE255810. Additional data that support the findings of this study are available from the corresponding author upon request.

ACKNOWLEDGMENTS

We thank Robbie L. Conley and Dr. Jun Wang for their expert technical assistance. The work was supported by a grant from the Friedreich's Ataxia Research Alliance to J.S.N. and grants from the National Institutes of Health National Institute of Neurological Disorders and Stroke (R01NS121038 to M.N. and R03NS099953 to J.S.N.).

AUTHOR CONTRIBUTIONS

S.M., L.P., J.S.N., and M.N. designed experiments; D.F., J.S.N., and J. Li provided critical reagents; S.M., L.P., and J.S.N. performed experiments; A.S. and J. Lee performed bioinformatic and statistical analyses; S.M., J.S.N., E.S., R.B.W., M.G.C., and M.N. interpreted results and advised experiments; J.S.N. and M.N. wrote the manuscript with input from all authors.

DECLARATION OF INTERESTS

E.S. is an employee of Friedreich's Ataxia Research Alliance, and M.N. and R.B.W. are members of the Friedreich's Ataxia Research Alliance scientific advisory board.

SUPPLEMENTAL INFORMATION

Supplemental information can be found online at https://doi.org/10.1016/j.omtm.2024.101347.

REFERENCES

1. Campuzano, V., Montermini, L., Moltò, M.D., Pianese, L., Cossée, M., Cavalcanti, F., Monros, E., Rodius, F., Duclos, F., Monticelli, A., et al. (1996). Friedreich's ataxia: autosomal recessive disease caused by an intronic GAA triplet repeat expansion. Science *271*, 1423–1427.

2. Durr, A., Cossee, M., Agid, Y., Campuzano, V., Mignard, C., Penet, C., Mandel, J.L., Brice, A., and Koenig, M. (1996). Clinical and genetic abnormalities in patients with Friedreich's ataxia. N. Engl. J. Med. *335*, 1169–1175. https://doi.org/10.1056/NEJM199610173351601.

3. Filla, A., De Michele, G., Cavalcanti, F., Pianese, L., Monticelli, A., Campanella, G., and Cocozza, S. (1996). The relationship between trinucleotide (GAA) repeat length and clinical features in Friedreich ataxia. Am. J. Hum. Genet. *59*, 554–560.

4. Cossee, M., Durr, A., Schmitt, M., Dahl, N., Trouillas, P., Allinson, P., Kostrzewa, M., Nivelon-Chevallier, A., Gustavson, K.H., Kohlschutter, A., et al. (1999). Friedreich's ataxia: point mutations and clinical presentation of compound heterozygotes. Ann. Neurol. *45*, 200–206.

5. Galea, C.A., Huq, A., Lockhart, P.J., Tai, G., Corben, L.A., Yiu, E.M., Gurrin, L.C., Lynch, D.R., Gelbard, S., Durr, A., et al. (2016). Compound heterozygous FXN

mutations and clinical outcome in friedreich ataxia. Ann. Neurol. *79*, 485–495. https://doi.org/10.1002/ana.24595.

6. Martelli, A., and Puccio, H. (2014). Dysregulation of cellular iron metabolism in Friedreich ataxia: from primary iron-sulfur cluster deficit to mitochondrial iron accumulation. Front. Pharmacol. *5*, 130. https://doi.org/10.3389/fphar.2014.00130.

7. Lynch, D.R., Chin, M.P., Boesch, S., Delatycki, M.B., Giunti, P., Goldsberry, A., Hoyle, J.C., Mariotti, C., Mathews, K.D., Nachbauer, W., et al. (2023). Efficacy of Omaveloxolone in Friedreich's Ataxia: Delayed-Start Analysis of the MOXIe Extension. Mov. Disord. *38*, 313–320. https://doi.org/10.1002/mds.29286.

8. Boesch, S., and Indelicato, E. (2024). Approval of omaveloxolone for Friedreich ataxia. Nat. Rev. Neurol. *20*, 313–314. https://doi.org/10.1038/s41582-024-00957-9.

9. Lynch, D.R., Goldsberry, A., Rummey, C., Farmer, J., Boesch, S., Delatycki, M.B., Giunti, P., Hoyle, J.C., Mariotti, C., Mathews, K.D., et al. (2024). Propensity matched comparison of omaveloxolone treatment to Friedreich ataxia natural history data. Ann. Clin. Transl. Neurol. *11*, 4–16. https://doi.org/10.1002/acn3.51897.

10. Zhang, S., Napierala, M., and Napierala, J.S. (2019). Therapeutic Prospects for Friedreich's Ataxia. Trends Pharmacol. Sci. *40*, 229–233. https://doi.org/10.1016/j.tips.2019.02.001.

11. Rocca, C.J., Rainaldi, J.N., Sharma, J., Shi, Y., Haquang, J.H., Luebeck, J., Mali, P., and Cherqui, S. (2020). CRISPR-Cas9 Gene Editing of Hematopoietic Stem Cells from Patients with Friedreich's Ataxia. Mol. Ther. Methods Clin. Dev. *17*, 1026–1036. https://doi.org/10.1016/j.omtm.2020.04.018.

12. Li, J., Rozwadowska, N., Clark, A., Fil, D., Napierala, J.S., and Napierala, M. (2019). Excision of the expanded GAA repeats corrects cardiomyopathy phenotypes of iPSC-derived Friedreich's ataxia cardiomyocytes. Stem Cell Res. *40*, 101529. https://doi.org/10.1016/j.scr.2019.101529.

13. Chang, J.C., Ryan, M.R., Stark, M.C., Liu, S., Purushothaman, P., Bolan, F., Johnson, C.A., Champe, M., Meng, H., Lawlor, M.W., et al. (2024). AAV8 gene therapy reverses cardiac pathology and prevents early mortality in a mouse model of Friedreich's ataxia. Mol. Ther. Methods Clin. Dev. *32*, 101193. https://doi.org/10.1016/j.omtm.2024.101193.

14. Clayton, R., Galas, T., Scherer, N., Farmer, J., Ruiz, N., Hamdani, M., Schecter, D., and Bettoun, D. (2024). Safety, pharmacokinetics, and pharmacodynamics of nomlabofusp (CTI-1601) in Friedreich's ataxia. Ann. Clin. Transl. Neurol. *11*, 540–553. https://doi.org/10.1002/acn3.51971.

15. United States Food and Drug Administration (2011). Potency tests for cellular and gene therapy products.FDA-2008-D-0520. https://www.fda.gov/regulatory-information/search-fda-guidance-documents/potency-tests-cellular-and-gene-therapy-products.

16. United States Food and Drug Administration (2023). Potency Assurance for Cellular and Gene Therapy Products.FDA-2023-D-4299. https://www.fda.gov/regulatory-information/search-fda-guidance-documents/potency-assurance-cellular-and-gene-therapy-products.

17. Lodi, R., Cooper, J.M., Bradley, J.L., Manners, D., Styles, P., Taylor, D.J., and Schapira, A.H. (1999). Deficit of in vivo mitochondrial ATP production in patients with Friedreich ataxia. Proc. Natl. Acad. Sci. USA *96*, 11492–11495. https://doi.org/10.1073/pnas.96.20.11492.

18. Chiang, S., Huang, M.L.H., Park, K.C., and Richardson, D.R. (2020). Antioxidant defense mechanisms and its dysfunctional regulation in the mitochondrial disease, Friedreich's ataxia. Free Radic. Biol. Med. *159*, 177–188. https://doi.org/10.1016/j.freeradbiomed.2020.07.019.

19. Chiang, S., Braidy, N., Maleki, S., Lal, S., Richardson, D.R., and Huang, M.L.H. (2021). Mechanisms of impaired mitochondrial homeostasis and NAD(+) metabolism in a model of mitochondrial heart disease exhibiting redox active iron accumulation. Redox Biol. *46*, 102038. https://doi.org/10.1016/j.redox.2021.102038.

20. Tamarit, J., Britti, E., Delaspre, F., Medina-Carbonero, M., Sanz-Alcázar, A., Cabiscol, E., and Ros, J. (2021). Mitochondrial iron and calcium homeostasis in Friedreich ataxia. IUBMB Life *73*, 543–553. https://doi.org/10.1002/iub.2457.

21. Monfort, B., Want, K., Gervason, S., and D'Autréaux, B. (2022). Recent Advances in the Elucidation of Frataxin Biochemical Function Open Novel Perspectives for the Treatment of Friedreich's Ataxia. Front. Neurosci. *16*, 838335. https://doi.org/10.3389/fnins.2022.838335.

22. Lengler, J., Coulibaly, S., Gruber, B., Ilk, R., Mayrhofer, J., Scheiflinger, F., Hoellriegl, W., Falkner, F.G., and Rottensteiner, H. (2020). Development of an In Vitro Biopotency Assay for an AAV8 Hemophilia B Gene Therapy Vector Suitable for Clinical Product Release. Mol. Ther. Methods Clin. Dev. *17*, 581–588. https://doi.org/10.1016/j.omtm.2020.03.013.

23. Perdomini, M., Hick, A., Puccio, H., and Pook, M.A. (2013). Animal and cellular models of Friedreich ataxia. J. Neurochem. *126*, 65–79. https://doi.org/10.1111/jnc.12219.

24. Li, Y., Polak, U., Clark, A.D., Bhalla, A.D., Chen, Y.Y., Li, J., Farmer, J., Seyer, L., Lynch, D., Butler, J.S., and Napierala, M. (2016). Establishment and Maintenance of Primary Fibroblast Repositories for Rare Diseases-Friedreich's Ataxia Example. Biopreserv. Biobank. *14*, 324–329. https://doi.org/10.1089/bio.2015.0117.

25. Crombie, D.E., Pera, M.F., Delatycki, M.B., and Pébay, A. (2016). Using human pluripotent stem cells to study Friedreich ataxia cardiomyopathy. Int. J. Cardiol. *212*, 37–43. https://doi.org/10.1016/j.ijcard.2016.03.040.

26. Schreiber, A.M., Misiorek, J.O., Napierala, J.S., and Napierala, M. (2019). Progress in understanding Friedreich's ataxia using human induced pluripotent stem cells. Expert Opin. Orphan Drugs *7*, 81–90. https://doi.org/10.1080/21678707.2019.1562334.

27. Maheshwari, S., Vilema-Enríquez, G., and Wade-Martins, R. (2023). Patient-derived iPSC models of Friedreich ataxia: a new frontier for understanding disease mechanisms and therapeutic application. Transl. Neurodegener. *12*, 45. https://doi.org/10.1186/s40035-023-00376-8.

28. Rodden, L.N., Chutake, Y.K., Gilliam, K., Lam, C., Soragni, E., Hauser, L., Gilliam, M., Wiley, G., Anderson, M.P., Gottesfeld, J.M., et al. (2021). Methylated and unmethylated epialleles support variegated epigenetic silencing in Friedreich ataxia. Hum. Mol. Genet. *29*, 3818–3829. https://doi.org/10.1093/hmg/ddaa267.

29. Nethisinghe, S., Kesavan, M., Ging, H., Labrum, R., Polke, J.M., Islam, S., Garcia-Moreno, H., Callaghan, M.F., Cavalcanti, F., Pook, M.A., and Giunti, P. (2021). Interruptions of the FXN GAA Repeat Tract Delay the Age at Onset of Friedreich's Ataxia in a Location Dependent Manner. Int. J. Mol. Sci. *22*, 7507. https://doi.org/10.3390/ijms22147507.

30. Masnovo, C., Lobo, A.F., and Mirkin, S.M. (2022). Replication dependent and independent mechanisms of GAA repeat instability. DNA Repair *118*, 103385. https://doi.org/10.1016/j.dnarep.2022.103385.

31. Matos-Rodrigues, G., van Wietmarschen, N., Wu, W., Tripathi, V., Koussa, N.C., Pavani, R., Nathan, W.J., Callen, E., Belinky, F., Mohammed, A., et al. (2022). S1-END-seq reveals DNA secondary structures in human cells. Mol. Cell *82*, 3538–3552.e5. https://doi.org/10.1016/j.molcel.2022.08.007.

32. Mincheva-Tasheva, S., Obis, E., Tamarit, J., and Ros, J. (2014). Apoptotic cell death and altered calcium homeostasis caused by frataxin depletion in dorsal root ganglia neurons can be prevented by BH4 domain of Bcl-xL protein. Hum. Mol. Genet. *23*, 1829–1841. https://doi.org/10.1093/hmg/ddt576.

33. Carletti, B., Piermarini, E., Tozzi, G., Travaglini, L., Torraco, A., Pastore, A., Sparaco, M., Petrillo, S., Carrozzo, R., Bertini, E., and Piemonte, F. (2014). Frataxin silencing inactivates mitochondrial Complex I in NSC34 motoneuronal cells and alters glutathione homeostasis. Int. J. Mol. Sci. *15*, 5789–5806. https://doi.org/10.3390/ijms15045789.

34. Shen, Y., McMackin, M.Z., Shan, Y., Raetz, A., David, S., and Cortopassi, G. (2016). Frataxin Deficiency Promotes Excess Microglial DNA Damage and Inflammation that Is Rescued by PJ34. PLoS One *11*, e0151026. https://doi.org/10.1371/journal.pone.0151026.

35. Chandran, V., Gao, K., Swarup, V., Versano, R., Dong, H., Jordan, M.C., and Geschwind, D.H. (2017). Inducible and reversible phenotypes in a novel mouse model of Friedreich's Ataxia. Elife *6*, e30054. https://doi.org/10.7554/eLife.30054.

36. Fil, D., Chacko, B.K., Conley, R., Ouyang, X., Zhang, J., Darley-Usmar, V.M., Zuberi, A.R., Lutz, C.M., Napierala, M., and Napierala, J.S. (2020). Mitochondrial damage and senescence phenotype of cells derived from a novel frataxin G127V point mutation mouse model of Friedreich's ataxia. Disease Models Mech. *13*, dmm045229. https://doi.org/10.1242/dmm.045229.

37. Fil, D., Conley, R.L., Zuberi, A.R., Lutz, C.M., Gemelli, T., Napierala, M., and Napierala, J.S. (2023). Neurobehavioral deficits of mice expressing a low level of

G127V mutant frataxin. Neurobiol. Dis. *177*, 105996. https://doi.org/10.1016/j.nbd.2023.105996.

38. Garcia-Gimenez, J.L., Gimeno, A., Gonzalez-Cabo, P., Dasi, F., Bolinches-Amoros, A., Molla, B., Palau, F., and Pallardo, F.V. (2011). Differential expression of PGC-1alpha and metabolic sensors suggest age-dependent induction of mitochondrial biogenesis in Friedreich ataxia fibroblasts. PLoS One *6*, e20666. https://doi.org/10.1371/journal.pone.0020666.

39. Zhao, H., Li, H., Hao, S., Chen, J., Wu, J., Song, C., Zhang, M., Qiao, T., and Li, K. (2017). Peptide SS-31 upregulates frataxin expression and improves the quality of mitochondria: implications in the treatment of Friedreich ataxia. Sci. Rep. *7*, 9840. https://doi.org/10.1038/s41598-017-10320-2.

40. Codazzi, F., Hu, A., Rai, M., Donatello, S., Salerno Scarzella, F., Mangiameli, E., Pelizzoni, I., Grohovaz, F., and Pandolfo, M. (2016). Friedreich ataxia-induced pluripotent stem cell-derived neurons show a cellular phenotype that is corrected by a benzamide HDAC inhibitor. Hum. Mol. Genet. *25*, 4847–4855. https://doi.org/10.1093/hmg/ddw308.

41. Li, J., Li, Y., Wang, J., Gonzalez, T.J., Asokan, A., Napierala, J.S., and Napierala, M. (2020). Defining transcription regulatory elements in the human frataxin gene: implications for gene therapy. Hum. Gene Ther. *31*, 839–851.

42. Elhamamsy, A.R., Metge, B.J., Alsheikh, H.A., Shevde, L.A., and Samant, R.S. (2022). Ribosome Biogenesis: A Central Player in Cancer Metastasis and Therapeutic Resistance. Cancer Res. *82*, 2344–2353. https://doi.org/10.1158/0008-5472.CAN-21-4087.

43. Aharon-Hefetz, N., Frumkin, I., Mayshar, Y., Dahan, O., Pilpel, Y., and Rak, R. (2020). Manipulation of the human tRNA pool reveals distinct tRNA sets that act in cellular proliferation or cell cycle arrest. Elife *9*, e58461. https://doi.org/10.7554/eLife.58461.

44. Zhang, Z., Ye, Y., Gong, J., Ruan, H., Liu, C.J., Xiang, Y., Cai, C., Guo, A.Y., Ling, J., Diao, L., et al. (2018). Global analysis of tRNA and translation factor expression reveals a dynamic landscape of translational regulation in human cancers. Commun. Biol. *1*, 234. https://doi.org/10.1038/s42003-018-0239-8.

45. Warburg, O. (1925). The metabolims of carcinoma cells. J. Cancer Res. *9*, 148–163.

46. Hinkle, P.C. (2005). P/O ratios of mitochondrial oxidative phosphorylation. Biochim. Biophys. Acta *1706*, 1–11. https://doi.org/10.1016/j.bbabio.2004.09.004.

47. Liberti, M.V., and Locasale, J.W. (2016). The Warburg Effect: How Does it Benefit Cancer Cells? Trends Biochem. Sci. *41*, 211–218. https://doi.org/10.1016/j.tibs.2015.12.001.

48. DeBerardinis, R.J., and Chandel, N.S. (2020). We need to talk about the Warburg effect. Nat. Metab. *2*, 127–129. https://doi.org/10.1038/s42255-020-0172-2.

49. Wang, Y., and Patti, G.J. (2023). The Warburg effect: a signature of mitochondrial overload. Trends Cell Biol. *33*, 1014–1020. https://doi.org/10.1016/j.tcb.2023.03.013.

50. Vazquez, A., Liu, J., Zhou, Y., and Oltvai, Z.N. (2010). Catabolic efficiency of aerobic glycolysis: the Warburg effect revisited. BMC Syst. Biol. *4*, 58. https://doi.org/10.1186/1752-0509-4-58.

51. Boroughs, L.K., and DeBerardinis, R.J. (2015). Metabolic pathways promoting cancer cell survival and growth. Nat. Cell Biol. *17*, 351–359. https://doi.org/10.1038/ncb3124.

52. Levine, A.J., and Puzio-Kuter, A.M. (2010). The control of the metabolic switch in cancers by oncogenes and tumor suppressor genes. Science *330*, 1340–1344. https://doi.org/10.1126/science.1193494.

53. Rotig, A., de Lonlay, P., Chretien, D., Foury, F., Koenig, M., Sidi, D., Munnich, A., and Rustin, P. (1997). Aconitase and mitochondrial iron-sulphur protein deficiency in Friedreich ataxia. Nat. Genet. *17*, 215–217. https://doi.org/10.1038/ng1097-215.

54. Gerber, J., Mühlenhoff, U., and Lill, R. (2003). An interaction between frataxin and Isu1/Nfs1 that is crucial for Fzxc e/S cluster synthesis on Isu1. EMBO Rep. *4*, 906–911. https://doi.org/10.1038/sj.embor.embor918.

55. Parent, A., Elduque, X., Cornu, D., Belot, L., Le Caer, J.P., Grandas, A., Toledano, M.B., and D'Autréaux, B. (2015). Mammalian frataxin directly enhances sulfur transfer of NFS1 persulfide to both ISCU and free thiols. Nat. Commun. *6*, 5686. https://doi.org/10.1038/ncomms6686.

56. Fox, N.G., Yu, X., Feng, X., Bailey, H.J., Martelli, A., Nabhan, J.F., Strain-Damerell, C., Bulawa, C., Yue, W.W., and Han, S. (2019). Structure of the human frataxin-bound iron-sulfur cluster assembly complex provides insight into its activation mechanism. Nat. Commun. *10*, 2210. https://doi.org/10.1038/s41467-019-09989-y.

57. Rouault, T.A. (2012). Biogenesis of iron-sulfur clusters in mammalian cells: new insights and relevance to human disease. Dis. Model. Mech. *5*, 155–164. https://doi.org/10.1242/dmm.009019.

58. Angulo, M.B., Bertalovitz, A., Argenziano, M.A., Yang, J., Patel, A., Zesiewicz, T., and McDonald, T.V. (2023). Frataxin deficiency alters gene expression in Friedreich ataxia derived IPSC-neurons and cardiomyocytes. Mol. Genet. Genomic Med. *11*, e2093. https://doi.org/10.1002/mgg3.2093.

59. Turchi, R., Sciarretta, F., Ceci, V., Tiberi, M., Audano, M., Pedretti, S., Panebianco, C., Nesci, V., Pazienza, V., Ferri, A., et al. (2023). Butyrate prevents visceral adipose tissue inflammation and metabolic alterations in a Friedreich's ataxia mouse model. iScience *26*, 107713. https://doi.org/10.1016/j.isci.2023.107713.

60. Sciarretta, F., Zaccaria, F., Ninni, A., Ceci, V., Turchi, R., Apolloni, S., Milani, M., Della Valle, I., Tiberi, M., Chiurchiù, V., et al. (2024). Frataxin deficiency shifts metabolism to promote reactive microglia via glucose catabolism. Life Sci. Alliance *7*, e202402609. https://doi.org/10.26508/lsa.202402609.

61. Zhang, C., Liu, J., Liang, Y., Wu, R., Zhao, Y., Hong, X., Lin, M., Yu, H., Liu, L., Levine, A.J., et al. (2013). Tumour-associated mutant p53 drives the Warburg effect. Nat. Commun. *4*, 2935. https://doi.org/10.1038/ncomms3935.

62. Ooi, A.T., and Gomperts, B.N. (2015). Molecular Pathways: Targeting Cellular Energy Metabolism in Cancer via Inhibition of SLC2A1 and LDHA. Clin. Cancer Res. *21*, 2440–2444. https://doi.org/10.1158/1078-0432.CCR-14-1209.

63. Love, M.I., Huber, W., and Anders, S. (2014). Moderated estimation of fold change and dispersion for RNA-seq data with DESeq2. Genome Biol. *15*, 550. https://doi.org/10.1186/s13059-014-0550-8.